# Spatio-spectral metrology at focus of ultrashort lasers: a phase-retrieval approach

Antonin Borot, Fabien Quere

Antonin Borot, Fabien Quere. Spatio-spectral metrology at focus of ultrashort lasers: a phase-retrieval approach. Optics Express, 2018, 26 (20), pp.26444. 10.1364/OE.26.026444 . cea-02277445

**Research Article** Vol. 26, No. 20 | 1 Oct 2018 | OPTICS EXPRESS 26444

Optics EXPRESS

# Spatio-spectral metrology at focus of ultrashort lasers: a phase-retrieval approach

**ANTONIN BOROT**[1,2] **AND FABIEN QUÉRÉ**[1,3]

[1] *LIDYL, CEA, CNRS, Université Paris-Saclay, CEA Saclay, 91191 Gif-sur-Yvette, France*
[2] *antonin.borot@cea.fr*
[3] *fabien.quere@cea.fr*

**Abstract:** The complete characterization of an ultrashort laser beam ultimately requires the determination of its spatio-temporal electric field $E(x, y, t)$, or its spatio-spectral counterpart $\tilde{E}(x, y, \omega)$. We describe a new measurement technique called INSIGHT, which determines $\tilde{E}(x, y, \omega)$, up to an unknown spatially-homogeneous spectral phase. Combining this information with a temporal measurement at a single point of the beam then enables the determination of the spatio-temporal field $E(x, y, t)$. This technique is based on the combination of spatially-resolved Fourier-transform spectroscopy with an alternate-projection phase-retrieval algorithm. It can be applied to any reproducible laser source with a repetition rate higher than about 0.1 Hz, relies on a very simple device, does not require any reference beam, and circumvents the difficulty associated with the manipulation of large beam diameters by working in the vicinity of the beam focus. We demonstrate INSIGHT on a 100 TW-25 fs laser, and use the measurement results to introduce new representations for the analysis of spatio-temporal/spectral couplings of ultrashort lasers.

**OCIS codes:** (320.7090) Ultrafast lasers; (120.3180) Interferometry; (320.7100) Ultrafast measurements.

## References and links

1. C. Rullière, ed., *Femtosecond Laser Pulses*, Advanced Texts in Physics (Springer, 2005).
2. I. A. Walmsley and C. Dorrer, "Characterization of ultrashort electromagnetic pulses," Adv. Opt. Photonics **1**, 308–437 (2009).
3. C. Iaconis and I. A. Walmsley, "Spectral phase interferometry for direct electric-field reconstruction of ultrashort optical pulses," Opt. Lett. **23**, 792–794 (1998).
4. R. Trebino and D. J. Kane, "Using phase retrieval to measure the intensity and phase of ultrashort pulses: frequency-resolved optical gating," J. Opt. Soc. Am. A **10**, 1101–1111 (1993).
5. T. Oksenhendler, S. Coudreau, N. Forget, V. Crozatier, S. Grabielle, R. Herzog, O. Gobert, and D. Kaplan, "Self-referenced spectral interferometry," Appl. Phys. B: Lasers Opt. **99**, 7–12 (2010).
6. M. Miranda, T. Fordell, C. Arnold, A. L'Huillier, and H. Crespo, "Simultaneous compression and characterization of ultrashort laser pulses using chirped mirrors and glass wedges," Opt. Express **20**, 688–697 (2012).
7. S. Aktürk, X. Gu, P. Gabolde, and R. Trebino, "First-order spatiotemporal distortions of Gaussian pulses and beams," Springer Ser. Opt. Sci. **132**, 233–239 (2007).
8. S. Akturk, X. Gu, P. Bowlan, and R. Trebino, "Spatio-temporal couplings in ultrashort laser pulses," J. Opt. **12**, 9 (2010).
9. G. Pariente, V. Gallet, A. Borot, O. Gobert, and F. Quéré, "Space-time characterization of ultra-intense femtosecond laser beams," Nat. Photonics **10**, 547–553 (2016).
10. E. Esarey, C. B. Schroeder, and W. P. Leemans, "Physics of laser-driven plasma-based electron accelerators," Rev. Mod. Phys. **81**, 1229–1285 (2009).
11. A. Macchi, M. Borghesi, and M. Passoni, "Ion acceleration by superintense laser-plasma interaction," Rev. Mod. Phys. **85**, 751–793 (2013).
12. F. Krausz and M. Ivanov, "Attosecond physics," Rev. Mod. Phys. **81**, 163–234 (2009).
13. H. Vincenti and F. Quéré, "Attosecond lighthouses: How to use spatiotemporally coupled light fields to generate isolated attosecond pulses," Phys. Rev. Lett. **108**, 113904 (2012).
14. G. Pariente and F. Quéré, "Spatio-temporal light springs: extended encoding of orbital angular momentum in ultrashort pulses," Opt. Lett. **40**, 2037–2040 (2015).
15. A. Sainte-Marie, O. Gobert, and F. Quéré, "Controlling the velocity of ultrashort light pulses in vacuum through spatio-temporal couplings," Optica **4**, 1298–1304 (2017).
16. G. Zhu, J. van Howe, M. Durst, W. Zipfel, and C. Xu, "Simultaneous spatial and temporal focusing of femtosecond pulses," Opt. Express **13**, 2153–2159 (2005).

#328341 https://doi.org/10.1364/OE.26.026444
Journal © 2018 Received 20 Apr 2018; revised 29 Aug 2018; accepted 29 Aug 2018; published 26 Sep 2018

17. H. E. Kondakci and A. F. Abouraddy, "Diffraction-free space-time light sheets," Nat. Photonics **11**, 733–740 (2017).
18. D. H. Froula, D. Turnbull, A. S. Davies, T. J. Kessler, D. Haberberger, J. P. Palastro, S.-W. Bahk, I. A. Begishev, R. Boni, S. Bucht, J. Katz, and J. L. Shaw, "Spatiotemporal control of laser intensity," Nat. Photonics **12**, 262–265 (2018).
19. P. Bowlan, P. Gabolde, A. Shreenath, K. McGresham, R. Trebino, and S. Akturk, "Crossed-beam spectral interferometry: a simple, high-spectral-resolution method for completely characterizing complex ultrashort pulses in real time," Opt. Express **14**, 11892–11900 (2006).
20. P. Gabolde and R. Trebino, "Single-shot measurement of the full spatio-temporal field of ultrashort pulses with multi-spectral digital holography," Opt. Express **14**, 11460–11467 (2006).
21. F. Bragheri, D. Faccio, F. Bonaretti, A. Lotti, M. Clerici, O. Jedrkiewicz, C. Liberale, S. Henin, L. Tartara, V. Degiorgio, and P. Di Trapani, "Complete retrieval of the field of ultrashort optical pulses using the angle-frequency spectrum," Opt. Lett. **33**, 2952–2954 (2008).
22. B. Alonso, Í. J. Sola, Ó. Varela, J. Hernández-Toro, C. Méndez, J. San Román, A. Zaïr, and L. Roso, "Spatiotemporal amplitude-and-phase reconstruction by fourier-transform of interference spectra of high-complex-beams," JOSA B **27**, 933–940 (2010).
23. S. L. Cousin, J. M. Bueno, N. Forget, D. R. Austin, and J. Biegert, "Three-dimensional spatiotemporal pulse characterization with an acousto-optic pulse shaper and a Hartmann–Shack wavefront sensor," Opt. Lett. **37**, 3291–3293 (2012).
24. M. Miranda, M. Kotur, P. Rudawski, C. Guo, A. Harth, A. L'Huillier, and C. L. Arnold, "Spatiotemporal characterization of ultrashort laser pulses using spatially resolved Fourier transform spectrometry," Opt. Lett. **39**, 5142–5145 (2014).
25. M. Rhodes, Z. Guang, J. Pease, and R. Trebino, "Visualizing spatiotemporal pulse propagation: first-order spatiotemporal couplings in laser pulses," Appl. Opt. **56**, 3024–3034 (2017).
26. M. Born, E. Wolf, A. B. Bhatia, P. C. Clemmow, D. Gabor, A. R. Stokes, A. M. Taylor, P. A. Wayman, and W. L. Wilcock, *Principles of Optics* (Cambridge University, 1999).
27. I. V. Il'ina, T. Y. Cherezova, and A. V. Kudryashov, "Gerchberg—Saxton algorithm: experimental realisation and modification for the problem of formation of multimode laser beams," Quantum Electron. **39**, 521–527 (2009).
28. L. Bruel, "Numerical phase retrieval from beam intensity measurements in three planes," Laser-Induced Damage Opt. Mater. **4932**, 590–598 (2003).
29. R. J. Bell and R. N. Bracewell, *Introductory Fourier Transform Spectroscopy*, vol. 41 (Academic Press, 1973).
30. N. Wiener, "Generalized harmonic analysis," Acta Math. **55**, 117–258 (1930).
31. A. Khintchine, "Korrelationtheorie der stationaren stochastischen Prozesse," Math. Annalen **109**, 604–615 (1934).
32. Note that for experiments using tight focusing (typically focal spot size $\lesssim 20\mu m$), the focus is usually too small to be directly resolved by a camera. In such cases, it needs to be re-imaged and magnified with a microscope objective: the interferometer is then inserted between this imaging optic and the camera. This was the configuration used for measurements presented here.
33. S. Ranc, G. Chériaux, S. Ferré, J.-P. Rousseau, and J.-P. Chambaret, "Importance of spatial quality of intense femtosecond pulses," Appl. Phys. B **70**, S181–S187 (2000).
34. P. Tournois, "Acousto-optic programmable dispersive filter for adaptive compensation of group delay time dispersion in laser systems," Opt. Commun. **140**, 245–249 (1997).
35. A. Jeandet, A. Borot, K. Nakamura, S. Jolly, W. Leemans, and F. Quéré, "Spatio-temporal characterization of a petawatt femtosecond laser," In preparation (2018).
36. Z. Bor, "Distortion of femtosecond laser pulses in lenses," Opt. Lett. **14**, 119–121 (1989).
37. M. Miranda, M. Kotur, P. Rudawski, C. Guo, A. Harth, A. L'Huillier, and C. L. Arnold, "Spatiotemporal characterization of ultrashort optical vortex pulses," J. Mod. Opt. **64**, S1–S6 (2017).
38. A. Denoeud, L. Chopineau, A. Leblanc, and F. Quéré, "Interaction of Ultraintense Laser Vortices with Plasma Mirrors," Phys. Rev. Lett. **118**, 033902 (2017).
39. A. M. Yao and M. J. Padgett, "Orbital angular momentum: origins, behavior and applications," Adv. Opt. Photonics **3**, 161–204 (2011).
40. M. Mori, A. Pirozhkov, M. Nishiuchi, K. Ogura, A. Sagisaka, Y. Hayashi, S. Orimo, A. Fukumi, Z. Li, M. Kado, and H. Daido, "Development of beam-pointing stabilizer on a 10-TW Ti:Al2O3 laser system JLITE-X for laser-excited ion accelerator research," Laser Phys. **16**, 1092–1096 (2006).
41. B. Alonso, M. Miranda, F. Silva, V. Pervak, J. Rauschenberger, J. San Román, Í. J. Sola, and H. Crespo, "Characterization of sub-two-cycle pulses from a hollow-core fiber compressor in the spatiotemporal and spatiospectral domains," Appl. Phys. B **112**, 105–114 (2013).
42. T. Witting, F. Frank, C. A. Arrell, W. A. Okell, J. P. Marangos, and J. W. Tisch, "Characterization of high-intensity sub-4-fs laser pulses using spatially encoded spectral shearing interferometry," Opt. letters **36**, 1680–1682 (2011).

---

## 1. Introduction

Ultrashort laser sources have now become major scientific tools, used in very different research fields ranging from femtochemistry to material science, high-precision frequency metrology, or plasma physics [1]. The development of these advanced light sources has been intimately coupled with progress in optical metrology. In particular, the ability, since the late 90's, to accurately measure the temporal evolution of the local electric field $E(t)$ of ultrashort pulses [2] has played a crucial role in the optimization and applications of these lasers. Such measurements, once at the forefront of optical metrology, can be now routinely achieved thanks to a variety of elegant techniques [3–6].

Yet, all laser beams unavoidably have a transverse spatial extent in the $(x, y)$ plane normal to the propagation direction $z$. Variations of the temporal/spectral properties of the pulse across this plane are called spatio-temporal/spectral couplings, and can be induced by even the simplest optical elements such as lenses, prisms or gratings [7]. Thus, the complete characterization of ultrashort laser beams actually requires measurement of the complex-valued electric field $E(x, y, t)$ in space-time, or equivalently of its counterpart $\tilde{E}(x, y, \omega)$ in space-frequency [8].

Fully determining this spatio-temporal/spectral electric field is crucial from several respects. First, by providing comprehensive information on the laser beam, it opens the way to unprecedented optimizations of its properties in 3D, which is essential for applications requiring the most advanced performances, e.g. in terms of peak intensity at focus [9] (for laser-driven particle acceleration [10, 11]) or of pulse duration (for single attosecond pulse generation [12]). Second, the interaction of these beams with matter often involves a collective response of the medium to the laser field, as well as a transverse and/or longitudinal 'coherent' build-up of the resulting secondary emissions (such as high-order harmonics or high-energy electrons), both ultimately determined by the full spatio-temporal field $E(x, y, t)$ and its evolution along $z$. Measuring this field and using this information as an input for simulation codes would thus open the way to a finer understanding of laser-matter interaction experiments. Finally, spatio-temporal metrology is a prerequisite to spatio-temporal shaping of laser beams, which has recently been identified as a powerful way to tailor the beam properties, and thus to achieve advanced control of these interactions [13–18].

Research on spatio-temporal/spectral measurement techniques for ultrashort lasers has become increasingly active in the last ten years, and several techniques have now been demonstrated [9, 19–24], based on different concepts such as spatially-resolved spectral interferometry [19, 22], spectrally-resolved spatial interferometry [20] or wavefront sensing [23]. Many of these should actually rather be considered as spatio-spectral techniques, which determine $\tilde{E}(x, y, \omega)$ up to an unknown spatially-homogeneous spectral phase. An additional temporal measurement, either of a reference beam (e.g. in SEA TADPOLE [19], its variant STARFISH [22], or STRIPED FISH [20]), or of the field at a single point of the beam to be characterized (e.g. in TERMITES [9, 24] or HAMSTER [23]), is then required to lift this unknown, after which the spatio-temporal field can be calculated by a Fourier-transform with respect to frequency.

It is a fact though that none of these techniques has become widespread yet, probably due to their complexity and the difficulty of implementing them on advanced laser systems. A less obvious, yet major difficulty is that analyzing and understanding the structure of spatio-temporal/spectral fields (3D complex-valued matrices) provided by such techniques is far from trivial [25]- much more challenging for instance than getting insight into the temporal structure of a pulse. This has also significantly contributed to keep this advanced metrology so far accessible to specialists only.

In this article, we present two advances on spatio-temporal/spectral metrology of ultrashort laser beams, which should contribute to make it accessible to a broader community of users. First, we introduce a new spatio-spectral measurement technique, called INSIGHT, applicable to any reproducible ultrafast laser source with a repetition rate higher than typically 0.1 Hz: this technique does not use any reference beam, is based on a measurement device of extreme simplicity, and measures the spatio-spectral $E$-field directly at laser focus, precisely where most laser-matter interactions take place. INSIGHT provides the laser spatio-spectral field $\tilde{E}(x, y, \omega)$, up to an unknown spatially-homogeneous spectral phase. Combining the information with a temporal measurement at a single point of the beam, the complete spatio-temporal field $E(x, y, t)$ can then be obtained.

We demonstrate this technique on a high-power femtosecond laser, and use the measurement results to introduce new and simple tools for the analysis of the spatio-temporal/spectral structure of ultrashort beams. In particular, we transpose one of the essential concepts of standard wavefront analysis, the Zernike polynomial decomposition of the spatial phase [26], to broadband laser sources. This representation provides a clear understanding of the nature of spatio-spectral couplings affecting broadband beams, and hence should prove very useful for the optimization of ultrashort lasers.

## 2. Principle

Let $\tilde{E}_{(z)}(x, y, \omega) = A_{(z)}(x, y, \omega)\, e^{i\phi_{(z)}(x,y,\omega)}$ be the complex electric field of the laser beam (assumed to be linearly-polarized) in the spatio-spectral domain at longitudinal position $z$, described by its spatio-spectral amplitude $A_{(z)}(x, y, \omega)$ (a real quantity) and spatio-spectral phase $\phi_{(z)}(x, y, \omega)$. The INSIGHT technique proceeds by first measuring $A_{(z)}(x, y, \omega)$ at different $z$ near focus, and then exploiting this information to numerically retrieve $\phi_{(z)}(x, y, \omega)$ (see Fig. 1).

An essential ingredient of the technique is thus the phase-retrieval procedure used in the second step. This is based on an adapted version of the well-known Gerchberg-Saxton (GS) iterative algorithm [27], which exploits the information encoded in the evolution of the spatial amplitude profile $A_{(z)}(x, y)$ of a monochromatic beam along the propagation axis $z$, to extract its spatial phase profile $\phi_{(z)}(x, y)$. The original GS algorithm uses amplitude profiles $A_{(z_i)}(x, y)$ measured in two planes related one to the other by a 2D spatial Fourier transformation: it retrieves the spatial phase by Fourier-transforming back and forth the complex field between these two planes, and imposing the measured amplitudes at each iteration step. In the present work, we use a variant where the spatial amplitudes are rather measured at and around the best focus of the beam, with typical distances between the measurement planes of several Rayleigh lengths $z_R$ [28]. In the iterative algorithm, the field is then propagated back and forth between these planes, using a plane wave decomposition in our case.

Although in principle strictly valid for monochromatic beams only, such algorithms are also commonly applied to broadband lasers, using as inputs the spectrally-integrated spatial profiles that are provided by cameras. This method is however doomed to fail for beams exhibiting significant spatio-spectral couplings: in such cases, the measured image is the incoherent sum over $\omega$ of different intensity profiles $A_{(z_i)}(x, y, \omega)$, and its evolution along $z$ can generally not be properly accounted for by the propagation of a single combination of spatial amplitude and phase profiles. The retrieval algorithm will then either converge to unphysical solutions, or not converge at all. The general idea can nonetheless be transposed to such beams by measuring the *spectrally-resolved* spatial amplitudes in different planes and then applying the retrieval algorithm separately *at each frequency of the spectrum* [21]. This is the first key idea of INSIGHT.

Different techniques can be considered to obtain the spectrally-resolved spatial amplitude profiles required for this phase retrieval procedure. One possibility is to use an imaging spectrometer with a 2D-detector, as in [21]. This however provides $A_{(z_i)}(x, y, \omega)$ along one spatial axis only, and thus restricts the approach to beams with cylindrical symmetry, or exhibiting STC in one spatial direction only, hence severely limiting its scope. Here, we avoid any assumption or limitation of this kind, by rather using *spatially-resolved* Fourier-transform spectroscopy. Widely used in different spectral ranges, this spectroscopic technique [29] relies on the Wiener-Khintchine theorem [30, 31], which states that the spectral intensity of a light source is given by the Fourier transform of its linear autocorrelation function with respect to the delay, $A^2(\omega) = FT^{(\tau)}\left\{\int dt\, E(t)\, E^*(t-\tau)\right\}$. In the visible or near-visible range, this technique is readily implemented with a 2D spatial resolution by using cameras for the measurement [9, 24]. This gives access to the local spectrum everywhere across the beam: the spectrally-resolved

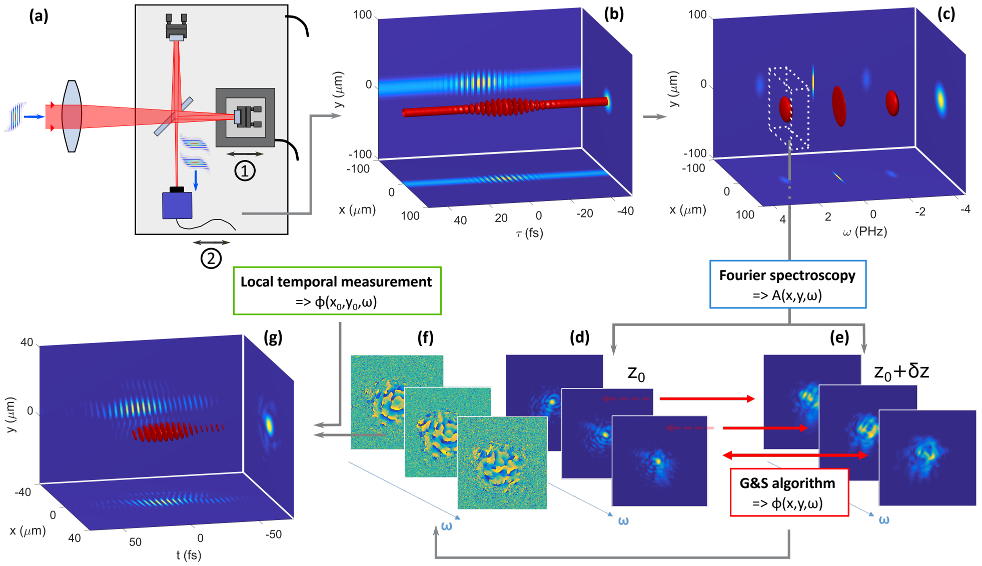

Fig. 1. Principle and implementation of INSIGHT. (a) The laser beam to be characterized is focused onto a 2D sensor placed at the output of a simple Michelson or Mach-Zehnder interferometer. A piezoelectric stage in one arm (stage 1 in (a)) is used to scan the delay with sub-optical-period accuracy, and thus measure the spatially-resolved linear autocorrelation of the beam at best focus (longitudinal position $z_0$), shown on (b). The Fourier transform of this signal with respect to delay (c) is then calculated, in order to filter out (white dashed box) the spatially-resolved spectrum $A_{(z_0)}(x, y, \omega)$. This 3D dataset provides the amplitude profiles at each frequency, shown in (d). This process is repeated at two other longitudinal positions near focus $z_0 \pm \delta z$ by shifting the interferometer (stage 2 in (a)), or equivalently the focusing or imaging optics, in the direction of the incoming beam, thus providing the spectrally-resolved spatial amplitudes $A_{(z_0 \pm \delta z)}(x, y, \omega)$ at $z_0 \pm \delta z$. For illustration, panel (e) displays $A_{(z_0+\delta z)}(x, y, \omega)$ only. A GS-like phase retrieval algorithm is then applied on each group of amplitudes in order to extract the spatial phase at each frequency, examples of which are shown in (f). INSIGHT provides the spatio-spectral field up to an unknown spatially-homogeneous spectral phase, since the measurement is blind to the evolution of phase with frequency. This unknown can be lifted by an independent measurement of the spectral phase at one position in the beam. Once this is done, a Fourier transformation with respect to $\omega$ is performed to obtain the field $E(x, y, t)$ in space-time, the real part of which is shown on (g).

spatial amplitude profiles are then directly obtained by taking spatial slices of this 3D dataset at each frequency.

The measurement device is very simple and easy to implement. It consists of a simple Michelson or Mach-Zender interferometer (see Fig. 1(a)) inserted between the focusing optic and the focal area [32]. The interferometer creates two replicas which recombine and overlap spatially with a controllable delay $\tau$ on a camera chip, leading a total signal given by $S(x, y, \tau) = \int dt\, |E(x, y, t) + E(x, y, t - \tau)|^2$. The delay is then scanned with sub-optical-cycle precision until the two replicas no longer overlap temporally, while images of the interference pattern are recorded on the camera. The resulting 3D signal (see Fig. 1(b)) contains the spatially-resolved linear-autocorrelation $c(x, y, \tau) = \int dt\, E(x, y, t)\, E^*(x, y, t - \tau)$ of the laser beam. This signal is selected by a Fourier-transformation of $S(x, y, \tau)$ with respect to $\tau$, followed by a filtering of the positive side peak (see Fig. 1(c)). This directly leads to the spectral intensity $A^2(x, y, \omega)$ for each position $(x, y)$ across the laser beam, with a spectral resolution inversely proportional to the temporal width of the delay scan. Examples of spectrally-resolved spatial amplitude profiles obtained in this way are shown in Fig. 1(d), for three frequencies in the laser bandwidth. The processing time required to extract this information from the raw images is of the order of a few minutes (one minute for each measurement plane in our case, using a standard laptop equipped with an Intel I7 2.7 GHz processor).

This measurement, first performed at or close to the best focus position $z_0$, is repeated at two other positions $z_0 + \delta z$ and $z_0 - \delta z$ before and after focus, for instance by shifting the measurement device along the laser propagation direction. This provides a triplet of spatio-spectral amplitudes at different longitudinal positions, $A_{(z_0)}(x, y, \omega)$ and $A_{(z_0 \pm \delta z)}(x, y, \omega)$ (see Fig. 1(d) and Fig. 1(e), where only two positions are shown for illustration). From these three 3D-matrices, we extract three spatial profiles at a single frequency $\omega$, that we use to seed our alternate projection phase-retrieval algorithm in order to determine the spatial phase $\phi_{(z_0)}(x, y, \omega)$ at this frequency. Using three spatial profiles rather than two greatly improves the stability and accuracy of the convergence [28]. The process is then repeated for each frequency within the laser spectral bandwidth, leading to a collection of spectrally-resolved spatial phase profiles, examples of which are shown in Fig. 1(f). The processing time required for this phase-retrieval algorithm to converge was about 5 minutes in our case, using the same laptop as before.

Since it provides all information on the spectral dependance of the spatial properties of the field, this procedure is sufficient to obtain all information on spatio-spectral couplings of the beam. However, since INSIGHT is totally insensitive to the relative phase between different frequencies, $\phi(x, y, \omega)$ is only retrieved up to a spatially-uniform spectral phase, which in particular prevents reconstructing the $E$-field in space-time. This missing information can be obtained through a single additional measurement, using a temporal measurement technique such as FROG [4] or SPIDER [3]. Such measurement is only required at one spatial position $(x_0, y_0)$ in the beam (provided all frequencies are present at this position [21]): once the local spectral phase $\phi(x_0, y_0, \omega)$ is known, the complete spatio-spectral phase $\phi(x, y, \omega)$ is obtained by imposing its spectral variation at $(x_0, y_0)$ -a process called frequency stitching. Temporal reconstruction is then possible by a Fourier-transform with respect to frequency.

This additional temporal measurement can in principle be done at focus, where the INSIGHT technique is applied, in which case performing frequency stitching is immediate. In practice, it is generally easier to perform a local temporal measurement on the collimated beam, before focusing. In this case, the spectrally-resolved fields provided by INSIGHT are first numerically propagated to this measurement plane. Frequency stitching is then achieved by imposing the spectral phase at position $(x_0, y_0)$ in this plane to match the value measured at this position. If needed, the beam can finally be propagated back to focus, so that the complete spatio-temporal electric-field at focus can be obtained, as shown in Fig. 1(g).

## 3. Results and analysis

In this section, we present the results of INSIGHT measurements performed on a high-power femtosecond laser, and use these results to address one of the difficulties that has hindered the development of spatio-temporal/spectral beam analysis so far: while the complex 3D matrix retrieved with techniques such as INSIGHT in principle contains all possible information on the laser $E$-field, in its raw form it does not readily shed light on the nature of the couplings affecting the beam. Deciphering this information requires the development of new specific representations associated to suitable visualization tools (see e.g. [25]). We will describe different such representations, which should at least partially cover the needs of both laser users and developers.

We applied the INSIGHT technique to the UHI100 laser system at CEA, delivering 100TW pulses of 25 fs duration with a spectrum centered at 800 nm, at a repetition rate of 10 Hz,

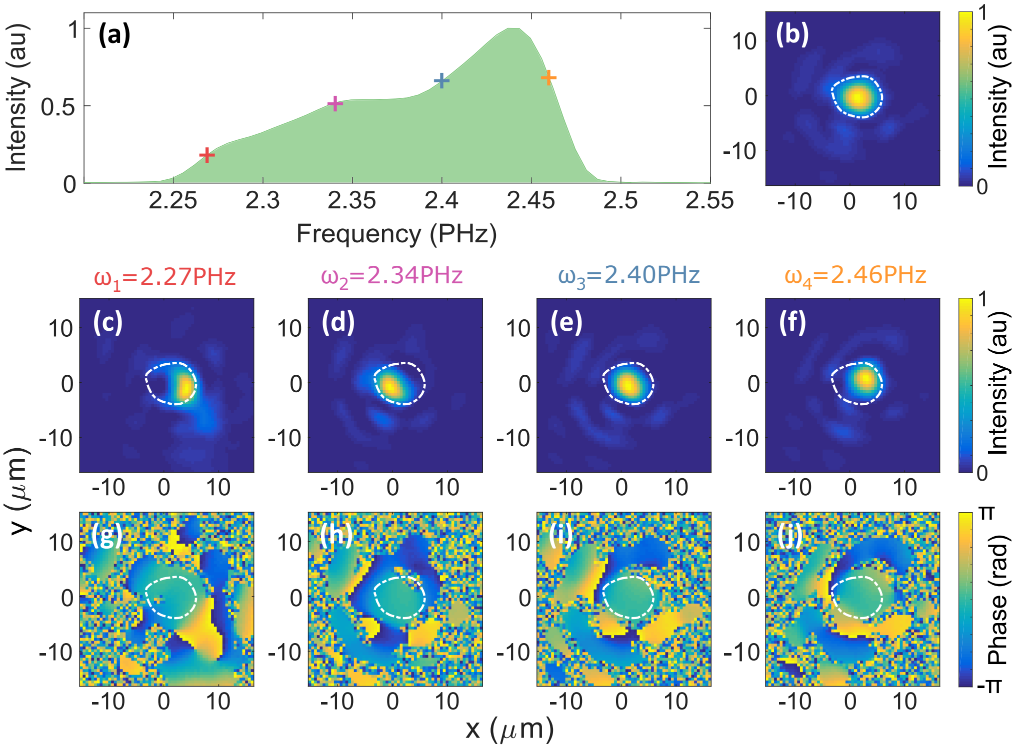

Fig. 2. Frequency-resolved spatial properties of the beam at best focus position $z_0$. Four frequencies $\omega_i$ are selected in the spatially-integrated spectrum (a), and the corresponding spatial intensities $A^2_{(z_0)}(x, y, \omega_i)$ (c-f) and phases $\phi_{(z_0)}(x, y, \omega_i)$ profiles (g-j) are shown. Panel (b) displays the frequency-integrated intensity profile (i.e. the focal spot), and the white lines in panels (c-j) its $1/e$ contour as a spatial reference.

in a beam of about 7 cm diameter. This laser was recently characterized in space-time, by implementing the self-referencing TERMITES technique [9] on the collimated beam (so-called near field). The beam was attenuated using neutral optical densities and/or uncoated wedges prior to the compressor. This attenuated beam was focused in the experimental chamber with the off-axis parabola used for the laser-plasma interaction experiments usually carried out with this laser, down to a focal spot of less than $5\mu m$ diameter (so-called far field). This focal spot was relay-imaged and magnified onto the camera of the INSIGHT device, outside of the vacuum chamber, with the same aberration-free microscope objective as used for focus optimization in usual experiments. The focal spot size was minimized using a deformable mirror [33], and the pulse duration was optimized on a small portion of the collimated beam using an acousto-optical modulator [34] (DAZZLER by FASTLITE). The feedback signals for these optimizations were respectively provided by frequency-integrated spatial measurements (a camera on the magnified focus and a wavefront sensor in the near-field) and spatially-localized temporal measurements (here carried out using self-referenced spectral interferometry [5] in the near field, i.e. WIZZLER by FASTLITE). The later also provided the phase information for frequency stitching of the INSIGHT data, required to then compute the field in the time domain.

### 3.1. Analysis of the beam properties in the far-field

The measurement of the spatio-spectral amplitude $A_{(z_0)}(x, y, \omega)$ at best focus - the very first step of INSIGHT measurements- already provides on its own highly valuable information on the beam

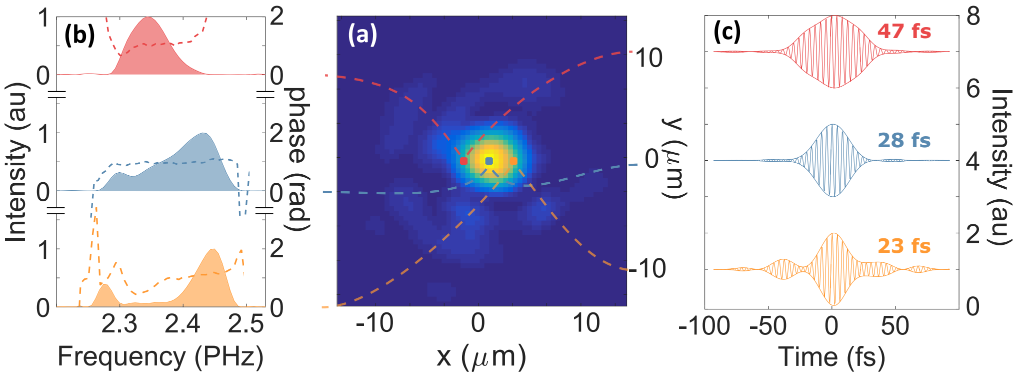

Fig. 3. Spatially-resolved spectral and temporal properties of the beam at focus. The frequency-integrated intensity profile (i.e. the focal spot) is shown in (a). The local spectral intensities $A^2(x_i, y_i, \omega)$ and phases $\phi(x_i, y_i, \omega)$ are shown in (b), for three positions $(x_i, y_i)$ across focus. The corresponding local temporal profiles are displayed in (c).

couplings. This is illustrated on Fig. 2(c)-2(f), which show the intensity profiles $A^2_{(z_0)}(x, y, \omega)$ for different laser frequencies $\omega_i$ $(i = 1 : 4)$. On each of these profiles, we indicated the $1/e$ contour of the frequency-integrated focal spot (shown in Fig. 2(b)) as a spatial reference. To first order, we observe a linear spatial drift of these spatial profiles from the bottom left to the top right for $\omega_2 \leq \omega \leq \omega_4$, with only slight changes in the beam profile -i.e. a linear spatial chirp resulting from angular dispersion in the near-field (see next subsection). In contrast, for the lowest frequencies around $\omega_1$, it gets distorted and moves back to the bottom right. This reveals that the beam experiences a combination of low order couplings, leading to the linear drift of focus position with frequency, and high order couplings, associated to the complex distortions of the beam profile.

The very same data can be analyzed from a different perspective, by now considering the local spectrum of the pulse as a function of position across focus. This is illustrated in Fig. 3(b), which displays this local spectrum at three positions along an horizontal line across focus, indicated on the frequency-integrated focal spot shown in Fig. 3(a) (same data as in Fig. 2(b)). An obvious consequence of the drift of the focal spot with frequency is that the spectrum suffers from significant spatial inhomogeneities. The spectrum at the center of the beam (blue) is broad and smooth, while the spectra on the sides (red and orange) are either narrow (top) or strongly structured (bottom). This will unavoidably results in spatial variations of the pulse duration. Determining these variations however requires the knowledge of the phase properties of the beam.

These phase properties are provided by the second step of the INSIGHT measurement procedure: the spatial phase profiles retrieved at four different frequencies are displayed in Fig. 2(g)-2(j). Such profiles at focus actually provide little intuitive insight into the beam properties. But by rather performing linouts of $\phi_{(z_0)}(x, y, \omega)$ along the frequency axis (after appropriate frequency stitching), we obtain the local spectral phase at each position in the beam, plotted in Fig. 3(b). The local pulse temporal profiles can then be calculated by a Fourier-transformation, as illustrated in Fig. 3(c). Important spatial variations of the temporal properties are observed, with the pulse duration changing from 23 to 47 $fs$. Therefore, in the present case, the widely-used assumption of a homogeneous temporal structure across focus is clearly inaccurate.

The knowledge of the spectrally-resolved spatial phase profiles at focus has another major interest: combined with the spectrally-resolved spatial amplitude profiles, this can be used to numerically propagate each frequency of the pulse in any $z$ plane before or after focus (e.g. using

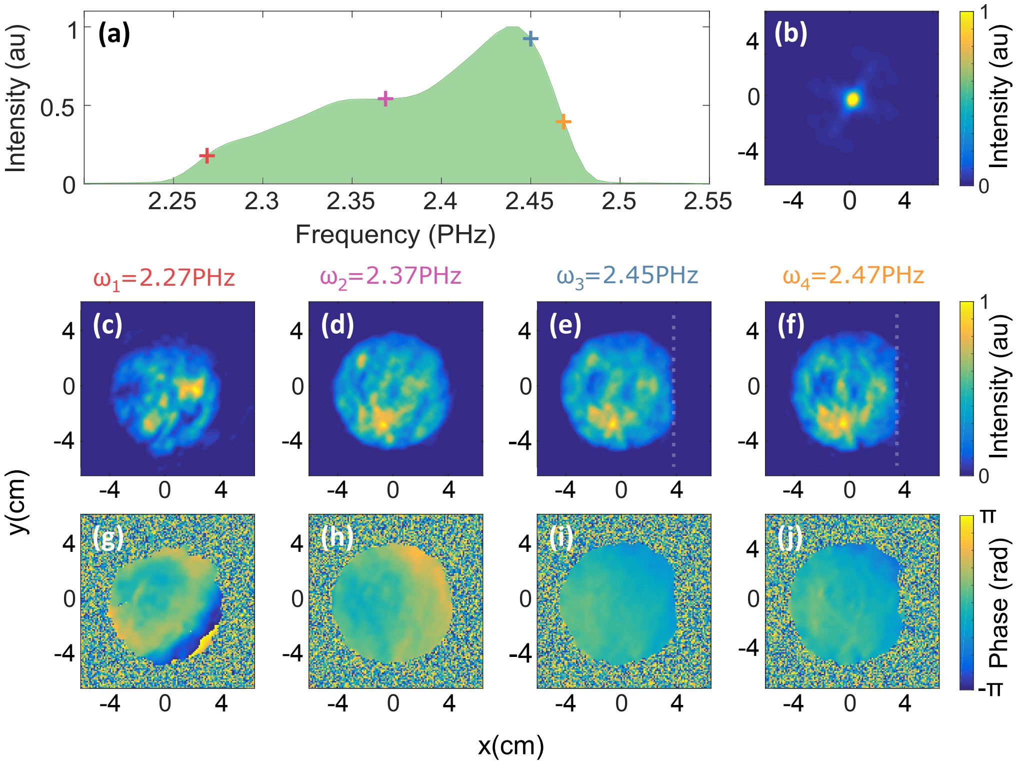

Fig. 4. Frequency-resolved spatial properties of the collimated laser beam. Four frequencies $\omega_i$ are selected in the spatially-integrated spectrum (a) and the corresponding spatial intensities $A^2_{(\infty)}(x, y, \omega_i)$ (c-f) and phases $\phi_{(\infty)}(x, y, \omega_i)$ (g-j) are shown. The vertical white dashed lines in panels (e-f) highlight the clipping of the beam at high frequencies. In (b) we show the calculated near-field spatial intensity at $\omega_2$ assuming a flat spatial phase at focus, to emphasize the importance of taking into account the actual spatial phase retrieved at focus.

plane wave decomposition), and then calculate the spatio-temporal $E$-field in this plane. The movie of the UHI100 laser pulse propagating through focus obtained in this way is provided in Visualization 1. This representation, as well as the ones of Fig. 2 and 3, are of prime interest to analyze the potential consequences of spatio-temporal/spectral couplings on laser-matter interaction experiments - for instance by using these data as inputs for simulation codes.

### 3.2. *Analysis of the beam properties in the near-field*

Based on this analysis in the far-field, it is however difficult to identify the physical nature and origin of the couplings affecting the beam. To this end, studying the structure of the beam in the near-field is more suitable. By now calculating the 2D spatial Fourier-transform of $\tilde{E}_{(z_0)}(x, y, \omega)$ for each $\omega$, the field structure $\tilde{E}_{(\infty)}(x, y, \omega)$ right after the focusing optics can be numerically deduced from the data of Fig. 2(c)-2(j). Here again, knowledge of the spatial phase (Fig. 2(g)-2(j)) is absolutely crucial. We illustrate this point by showing in Fig. 4(b) the near-field intensity profile obtained at frequency $\omega_2$ when assuming a flat spatial phase at focus. This profile is then totally different from what is expected: it is dominated by a very bright central spot of very small size, surrounded by a broader faint halo that matches the known diameter of the collimated beam.

This 'coherent artefact' obviously disappears when the actual spatial phase profiles measured at focus are taken into account: the reconstructed intensity profiles obtained at different frequencies

(Fig. 4(c)-4(f)) are now round and show the modulated super-gaussian shape typical of such lasers in the near-field, with the expected diameter. But much finer features are also recovered: for $\omega_3$ and $\omega_4$, the intensity profiles suffer from a vertical clip on the right edge of the beam, which drifts towards the center of the beam when frequency increases (see white dashed lines in Fig. 4(e) and 4(f)). As far as near-field phase profiles are concerned (Fig. 4(g)-4(j)), the most striking effect is the appearance of a localized aberration on the bottom right edge of the beam at frequency $\omega_1$, which qualitatively explains the observed degradation of the focal spot in this frequency range (Fig. 2(c)).

These amplitude and phase couplings are similar to the ones previously observed on UHI100 with TERMITES [9], which had been attributed to faulty optical elements and accidental beam clipping in the section of the compressor where the beam is spatially chirped -issues that have now been solved thanks to these new diagnostics. This provides a first qualitative validation of the INSIGHT technique, indicating that even subtle information on spectrally-dependent structures of the collimated beam is properly retrieved by INSIGHT, through its imprint on the frequency-resolved amplitude profiles around focus.

In this specific case, the comparison between the results provided by these two techniques can however not be quantitative. Indeed, for practical reasons, they had to be implemented at very different locations of the laser beam line, and were separated by more than a year. The TERMITES measurements were carried out right at the compressor output, while for the INSIGHT measurements, the beam had to further propagate over several meters, go through a double plasma mirror, a deformable mirror system, and reflect on all the optics of the experimental chamber, thus making a direct comparison both difficult and irrelevant. More straightforward and quantitative tests of INSIGHT will be described later in this section. Furthermore, a more recent measurement campaign performed with these two techniques around the same location of the BELLA laser beamline at LBNL (USA) demonstrated an excellent agreement [35].

We will now show that, beyond the peculiar high-order phase aberration observed at frequency $\omega_1$, the beam also suffers from lower-order chromatic aberrations, which are not as readily identified on the spatial phase profiles of Fig. 4(g)-4(j). Revealing these couplings requires the use of more advanced analysis tools. In standard wavefront analysis for monochromatic beams, spatial aberrations are usually identified by decomposing the phase profile as a linear superposition of Zernike polynomials, where each term of the superposition can be associated to a specific type of wavefront distortion, often resulting from known optical effects (e.g. misalignment of a lens). Here, we extend this analysis to broadband laser beams, by performing this decomposition independently at each frequency, and then plotting the obtained coefficients as a function of frequency, to get an immediate insight into the chromatic aberrations affecting a beam. We note that, in a similar way, time-resolved Zernike decompositions can also be carried out, in order to analyze the spatio-temporal phase properties of complex beams.

The results of this analysis for the UHI100 laser beam are presented in Fig. 5, for the five lowest aberration orders (from wavefront tilt to astigmatism), and illustrate its potential to reveal the nature and identify the origin of the chromatic abberations affecting broadband beams. The most striking feature is a quasi-linear change of the Zernike coefficients for $2.35\,PHz \leq \omega \leq 2.5\,PHz$. The strongest variation is for the horizontal wavefront tilt (green): this corresponds to a well-identified space-frequency phase-coupling known as angular dispersion [7], that leads to the horizontal spatial chirp observed at focus [13]. It can easily be compensated by adjusting the relative angle between gratings in the compressor. At the next order, we observe a linear variation of the wavefront curvature (white), another known coupling leading to pulse front curvature in space-time, and to longitudinal chromatism around focus [15, 36]. This typically results from the use of chromatic lenses in the laser system. The beam also has a non-zero frequency-averaged astigmatism with a slight dependence in frequency (orange and red): such coupling has never been reported to date to the best of our knowledge, and its origin is more difficult to identify.

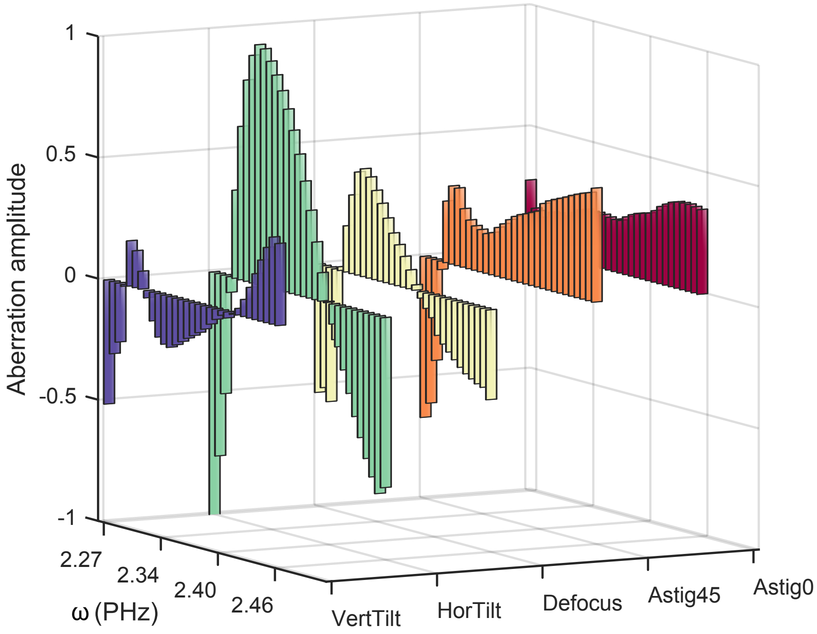

Fig. 5. Decomposition of the near-field spectrally-resolved spatial phase $\phi_{(\infty)}(x, y, \omega)$ onto the basis of Zernike polynomials. The five first polynomial coefficients (horizontal and vertical tilts, defocus, 45° and 0° astigmatisms) are showed, apart from the spectrally-resolved piston, which corresponds to the spatially-averaged spectral phase.

Much faster changes of the Zernike coefficients occur for $2.25\,PHz \leq \omega \leq 2.35\,PHz$. These are most likely due to the high-frequency distortion of the spatial phase occurring in this frequency range (see Fig. 4(g)), which cannot be properly described by a low-order Zernike polynomial decomposition.

### 3.3. Validation test and measurement of shaped beams

This frequency-resolved wavefront analysis is also useful to display a basic validation test of the measurement technique. In Fig. 6, we plot the variation with frequency of one of these Zernike coefficients, the horizontal tilt, obtained from two different INSIGHT measurements performed on UHI100. Between these two measurements, one of the gratings of the compressor was rotated by a small angle ($16 \times 10^{-3} deg$) around its vertical axis, in order to induce an angular dispersion in the horizontal plane, with an expected value of $3.3 \times 10^{-5} deg/nm$, which adds up to the small residual angular dispersion the beam already had. Subtracting these two curves, we indeed find a linear variation of this horizontal tilt with frequency, with a value of $3.4 \times 10^{-5} deg/nm$ very close to the expected one. The spatial wavefronts retrieved by INSIGHT at different frequencies in these two cases, as well as their differences, are presented in the supplementary material.

Finally, as emphasized in the introduction, one of the ultimate interests of spatio-temporal metrology is to characterize structured laser beams, that have been intentionally shaped to get specific physical effects, as was recently achieved in [37]. To test the capability of INSIGHT to measure more complex beams, we have introduced a stepped spiral phase plate (8 levels) in the UHI100 laser beam, in order to create a Laguerre-Gaussian beam of index $\ell = 1$ at $800\,nm$ [38, 39]. The reconstructed spatio-temporal $E$-field at focus is presented in Fig. 7, and clearly shows the expected helical wavefronts of the field. The measurement reveals that this is combined with a slight temporal wavefront rotation along $y$ (see back panel in Fig. 7), indicating

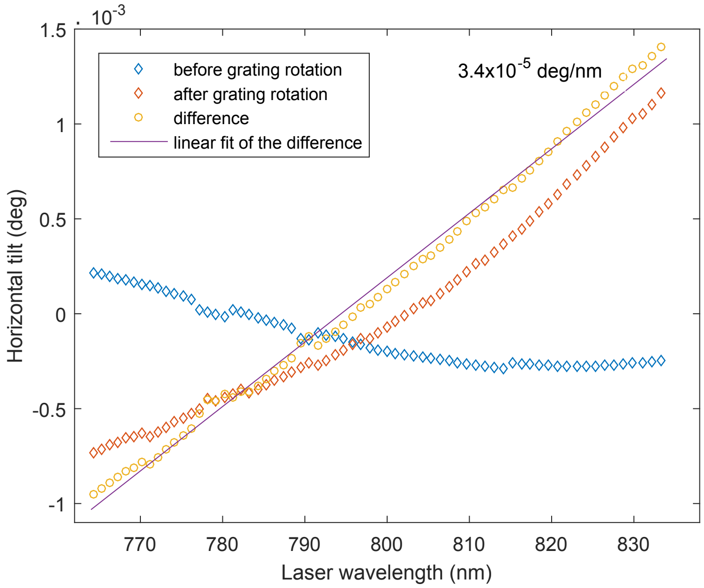

Fig. 6. Horizontal tilt as a function of frequency for UHI100, before and after a small rotation of one of the compressor gratings around its vertical axis. The rotation angle of $16 \times 10^{-3}$ degrees is expected to lead to a change in angular dispersion of $3.3 \times 10^{-5} deg/nm$. Subtracting the two curves leads to a measured value of $3.4 \times 10^{-5} deg/nm$, very close to the expected one.

the presence of a residual spatial chirp at focus, as observed in the previous measurements. Because of this undesired additional coupling, the doughnut beam profiles formed at focus by different frequencies are not perfectly overlapped transversely: this will result in a blurring of the frequency-integrated intensity ring formed by the broadband Laguerre-Gaussian beam. This illustrates the level of insight and ultimately optimization that can be provided by complete spatio-temporal/spectral metrology.

## 4. Discussion and comparison with TERMITES

The INSIGHT technique has many advantages. First, the experimental setup is very basic since it consists of a simple interferometer. Second, by working at focus, it avoids the considerable difficulties associated with the manipulation of very large beam diameters, such as those provided by high-power laser systems: a compact measurement device can be placed at the focal point used for laser-matter experiments, or in a corresponding image plane. This will facilitate the future characterization of PetaWatt femtosecond lasers, which have beam diameters of several tens of centimeters prior to focusing. Third, it does not require a reference beam, which is often difficult to produce, especially for high-power or ultrabroadband beams.

The proper implementation of INSIGHT however requires careful attention on several points, which are further detailed in the appendices. First, measurements of autocorrelation functions rely on a very accurate control of the position of the delay stage (typically better than $\lambda/80$, where $\lambda$ is the central wavelength, see Appendix A). This is achieved here by using high-quality piezoelectric stages, and also ensuring a good mechanical stability of the interferometer. The second difficulty is to handle the beam pointing instability, especially on high-power lasers where shot-to-shot displacements of the focal spot can easily get comparable to the spot size [40]: in such cases, each camera pixel will see a different part of the beam on different laser shots, thus potentially

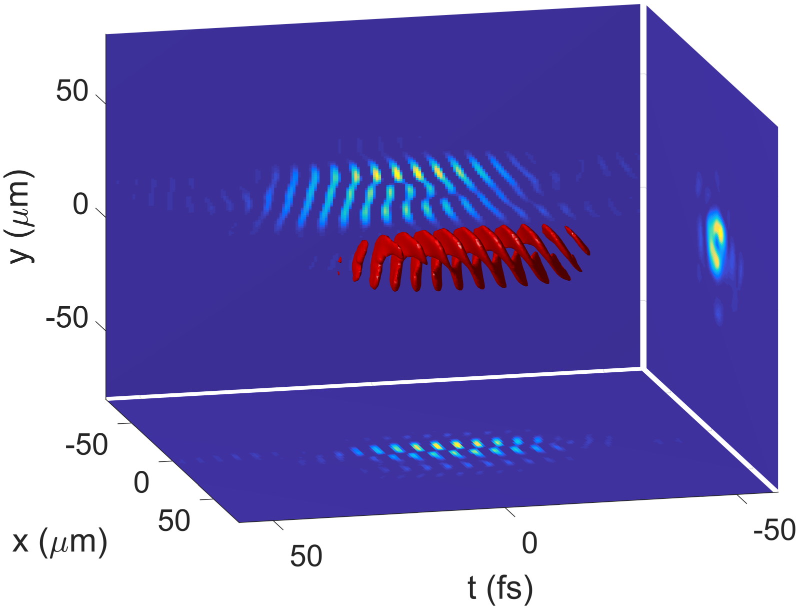

Fig. 7. Measured spatio-temporal $E$-field of the UHI100 laser when a $\ell = 1$ helical phase plate is introduced into the beam. See Visualization 2 for multiple perspectives. The carrier frequency has been numerically reduced by 50 % for the sake of visibility. This is why two intertwined helices are observed on the wavefront, although $\ell = 1$.

distorting the measured auto-correlation function and corrupting the retrieved spatio-spectral amplitudes. Different methods can be used to numerically eliminate these pointing fluctuations by post-processing of the images (see Appendix B). Finally, since the method requires many laser shots (typically a thousand for the measurements presented below), it of course applies to laser sources that are reproducible from shot-to-shot, and its implementation remains tractable only for repetition rates higher than 0.1 Hz typically, .

It is instructive to compare INSIGHT to the recently-introduced TERMITES technique [9, 24]. Both techniques use simple interferometers and rely on the general principle of Fourier-transform spectroscopy, and might thus appear similar at first sight. However, their principles are actually extremely different. As explained above, in INSIGHT, the interfering beams are identical replicas of the unknown beam, and the delay scan thus provides the spatially-resolved linear autocorrelation function of the beam, from which the spatially-resolved spectral intensity is derived. This is different in TERMITES, where the interfering beams are, on the one hand, the unknown beam, and on the other hand, a radially-stretched version of this beam, used as a self-reference: the temporal scan then provides the spatially-resolved linear cross-correlation function between these two beams, from which their spatially-resolved cross-spectral density function is obtained. The key difference between the two techniques lies in the way in which the spatio-spectral phase properties of the unknown beam are then deduced from these interferometric measurements. In TERMITES, this phase information is directly contained in the phase of the measured cross-spectral density function. In contrast, in INSIGHT, it is rather encoded in the evolution of the spatio-spectral amplitude profile of the beam along the propagation direction, from which it is extracted through the phase-retrieval procedure explained earlier.

These two techniques also have major practical differences, which make them complementary for the characterization of ultrashort lasers. Since TERMITES applies to collimated beams, it can easily be implemented at any point of complex laser systems, to track the origin of chromatic aberrations. On the other hand, implementing TERMITES on beams of very large diameter (typically $>$ 10 cm) gets very challenging because of the size of the optics, the size and resolution of the required sensor, and the involved propagation distance after the interferometer. In contrast, INSIGHT is best implemented near a focus, such that the beam spatial profile has a fast enough evolution along the propagation direction. As a result, it totally avoids the issues associated to large beam diameters, and can be based on a much more compact device than TERMITES. As will be explained in a future publication, the spatial resolution on the near-field spatio-spectral beam profiles numerically reconstructed from INSIGHT measurements however tends to be weaker than those obtained from TERMITES -which intrinsically have extremely high spatial-resolution. Of course, neither of these techniques are restricted to high-power laser systems, and we have already used them to perform measurement campaigns on less powerful lasers, which also revealed significant spatio-temporal couplings. Like several previous techniques [24, 37, 41, 42] as well as TERMITES, applying INSIGHT to few-cycles pulses is possible. In this case though, the final complementary phase stitching procedure will require special care, due to the extreme sensitivity of these pulses to even very small amounts of dispersion.

## 5. Conclusion

In conclusion, we have introduced a new technique for the complete spatio-temporal/spectral characterization of ultrashort lasers, where the measurement is performed near a focus, and the phase information is retrieved by a phase-retrieval approach. We have demonstrated this technique on a 100 TW laser, and used the measurement results to introduce different representations and analysis tools that can be exploited to shed light on the properties of ultrashort beams, from the perspective of both laser users and laser developers. A variety of techniques are now available for spatio-temporal/spectral measurements of ultrafast lasers, and more will very likely emerge in the coming years. Finding appropriate data analysis tools to get a clear understanding of the properties of the retrieved 3D complex fields is essential: the new ideas that have been introduced here on this issue can be applied whatever measurement technique is implemented, and will thus be of general use in ultrafast optics.

## 6. Appendix A: Importance of the delay step resolution in the interferometric scan

Spectral measurements using Fourier transform spectroscopy are known to require a precise control and diagnostic on the step size of the interferometric scan. To quantify this requirement, we consider a laser pulse with a spectrum centered at $\omega_0 = 2.35\, PHz$ ($\lambda = 800\, nm$) and spanning over $0.4\, PHz$, and we simulate the autocorrelation function of this pulse obtained delay steps exhibiting different amounts of noise. Figure 8 presents a comparison between the actual spectral intensity of the simulated pulse (red curve), and the spectral intensities (right column) retrieved by Fourier transformed spectroscopy (blue curve) for different amounts of noise on the step size. On top, we simulate a precise scan, with almost constant steps of $1\, fs$ over $800\, fs$ and a standard deviation of $0.04\, fs$ on the step size, which correspond to precision on the piezo stage of about $6\, nm$. The retrieved spectrum maps well the spectrum of the simulated light source. In the middle, we simulate a scan with steps exhibiting a standard deviation of $0.2\, fs$ ($30\, nm$ precision on the stage): the retrieved spectrum already shows an important deviation from the source spectrum. Finally we simulate a scan with steps with standard deviation of $0.4\, fs$ ($60\, nm$ precision on the stage), and we retrieve a strongly distorted spectrum. We therefore conclude that for measurements at $800\, nm$, a precision of the order of $5\, nm$ on the step size of the scan is ideal, and $10\, nm$ is satisfactory. For our experimental set-up and in our measurement conditions, we measured that the accuracy on the step size was of the order of $10\, nm$.

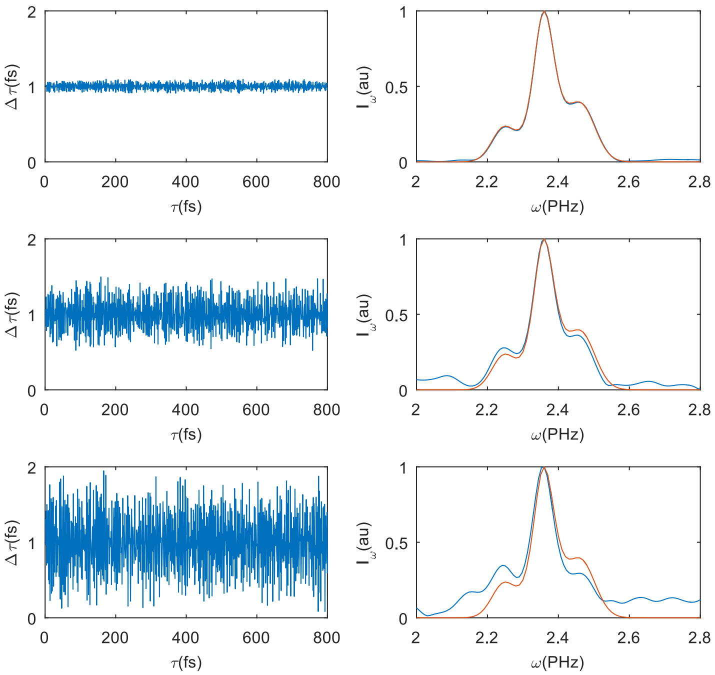

Fig. 8. Effect of the step size precision on the retrieved spectrum in Fourier-transform spectroscopy. We show here the results of simulations for different amounts of noise on the step size of the interferometric scan. The laser is centered at 800 $nm$ (optical period 2.7 $fs$). On the left column is the step size variation along the scan (RMS deviation of 0.04 $fs$, 0.2 $fs$ and 0.4 $fs$ from top to bottom), and on the right the original spectrum in red, and the spectra deduced from the autocorrelations in blue.

## 7. Appendix B: Numerical correction of the laser pointing jitter

Fourier-transform spectroscopy consists in retrieving the spectrum of a light source by calculating the Fourier transformation of its autocorrelation function. In the INSIGHT setup, this spatially-resolved autocorrelation function is experimentally obtained at and around focus by creating two replicas of the laser beam with an interferometer, and measuring their interference pattern on a camera sensor as a function of the delay. However, if the beam pointing exhibits strong shot-to-shot instabilities, the laser focal spot moves from one shot to the next, and the measured function is no longer the "pure" autocorrelation function, since any given camera pixel sees different parts of the beam for different delays. In Fig. 9(a), we show the spatially-resolved autocorrelation function (only the horizontal spatial direction is shown, the graph is taken for $y = 0$) recorded at focus of UHI100. We see that the fluctuations of the focal spot position are rather large, of the order of the spot size. Figure 9(b) shows the signal measured at ($x = 0$, $y = 0$), i.e. at the center of the beam: due to the beam position variation, the signal is strongly distorted, so that it is even difficult to distinguish the temporal overlap of the two replicas. As a result, the retrieved spectrum at ($x = 0$, $y = 0$), shown in Fig. 9(c), is noisy and slightly distorted due to a significant amount of white noise.

In order to improve the quality of the retrieved spatially-resolved spectrum, the fluctuations of the beam position on the sensor, resulting from the laser pointing jitter, can be numerically corrected after acquisition, by simply re-centering the consecutive acquired images. In the present case, this simple numerical processing however requires special care: it cannot be performed directly on the measured interference patterns, especially around the zero-delay between the

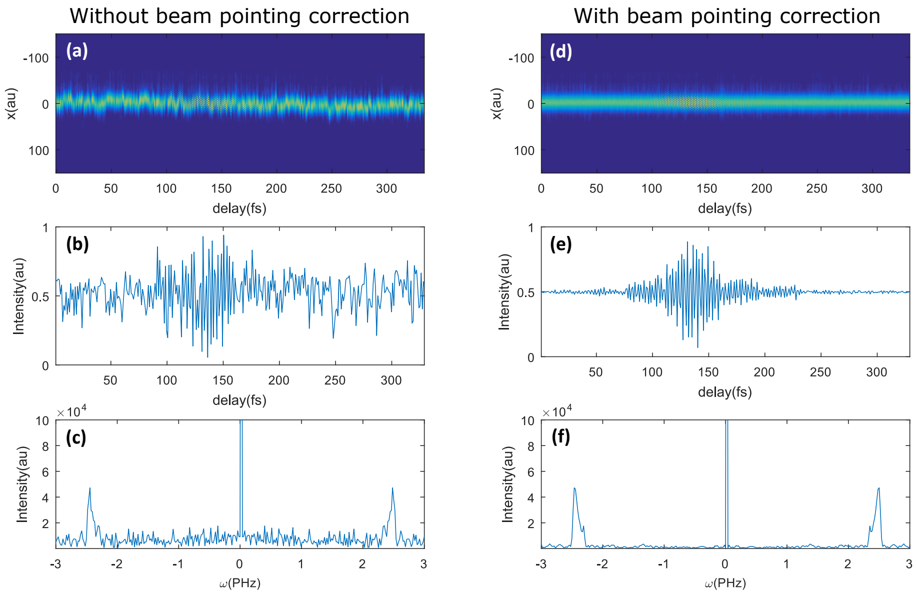

Fig. 9. Effect of the beam pointing jitter on the quality of the spectrum retrieved by spatially-resolved Fourier spectroscopy. The data shown here are taken on the UHI100 laser system and the results presented in the paper are extracted from these. Panel (a) presents a raw spatially-resolved interferometric scan (for readability purpose, only a cut at $(x, y = 0, \tau)$ is shown). The significant beam pointing jitter leads to a noisy and distorted autocorrelation function (see panel (b), which shows the signal at $(x = 0, y = 0)$ and a function of $\tau$). As a consequence, the corresponding retrieved spectrum (panel (c)) is affected by noise. Panel (d) presents the spatially-resolved interferometric scan after numerical correction of the beam position fluctuations, obtained from (a). The interferometric scan is then much cleaner, symmetric and contrasted (e) and the retrieved spectrum now presents a good signal-to-noise ratio (f).

replicas (which is where the useful signal lies). Indeed, the shape of the interference pattern might vary with the delay, making the numerical re-centering by image comparison unreliable. Different methods can be used to overcome this difficulty. A basic one is to collect a small fraction of the beam with a beam splitter prior to the interferometer, and to measure the position fluctuations at focus on this beam, with a second camera. Another option, which only requires one camera and that we have used in the present work, consists in introducing high-frequency spatial fringes in the interferograms (i.e. many spatial fringes within the beam focal spot), in such a way that the effect of interferences can be Fourier-filtered before numerical correction of the beam position. We detail the principle of this method in the next paragraph.

For this purpose, we use a Mach-Zehnder interferometer rather than a Michelson interferomer, in order to introduce a small angle in between the two replicas (see Fig. 10(a)) while maintaining a perfect spatial overlap on the camera (i.e. no spatial shearing between the replicas). The angle is introduced on the fixed arm, in order to avoid a walk-off of the replicas on the detector during the scan. This new configuration creates parallel interference fringes (see Fig. 10(b)) on top of the beam intensity profile. We then perform a 2D Fourier transformation of the beam intensity profile. The amplitude of the Fourier-transform, shown in Fig. 10(c), exhibits three patterns: the central one corresponds to the Fourier transform of the beam profile without interference fringes, and the two side patterns are its replicas centered at the spatial frequency of the spatial fringes. We see here that if the spatial frequency of the spatial fringes is higher than the maximum spatial

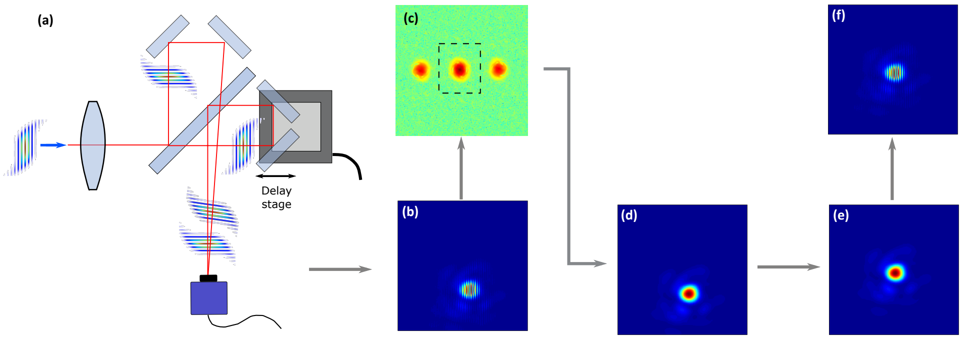

Fig. 10. Beam pointing numerical stabilization using a Mach-Zehnder interferometer (panel (a)). The two replicas spatially overlap on the camera with an angle. As a result, the intensity profile exhibits parallel spatial fringes (b). If the spatial period of the fringes is smaller than the shortest spatial pattern within the beam profile, the 2D-spatial Fourier transform (c) has three well separated peaks, the central one corresponding to the incoherent sum of the replicas' intensity profile. After filtering this central peak and Fourier-transforming back to the real space, the intensity profile is now free from spatial fringes (d), and its drift due to beam pointing jitter can be accurately calculated (e). This measured drift is then used to numerically correct the spatial position of the total interferometric signal (f), before performing the numerical processing described in the main text.

frequency of the beam intensity profile, then we can select only the central peak, and perform an inverse Fourier transformation back to the initial space. The intensity profile is then free from spatial interference fringes, as show in Fig. 10(d), and corresponds to incoherent sum of the intensity profiles of the two replicas -a signal that is totally independent of the delay between the replicas. It is then very easy to calculate the amount of spatial drift with respect a reference position, for instance the center of the image (see Fig. 10(e)), which we can then compensate on the measured intensity profiles *with inferferences* (see Fig. 10(f)). The resulting interferogram with numerical correction of the position fluctuations is shown on Fig. 9(d). The signal taken at the center of the image (Fig. 9(e)) now shows a much cleaner and symmetric autocorrelation function, and the retrieved spectrum is now almost noise-free, and identical to what can be measured with a spectrometer.

## 8. Appendix C: Measurement of induced controlled angular dispersion

Figure 11 displays the frequency-resolved wavefronts of the collimated UHI100 laser beam at four different frequencies, measured with INSIGHT before (upper line) and after (middle line) a rotation of a compressor grating by $16 \times 10^{-3}$ degrees. For these measurements, the deformable mirror located before the experimental chamber was intendedly not optimized, resulting in the distorted wavefronts observed on these measurements. Such distorted wavefronts are known to make it very difficult to detect residual angular dispersion on a beam by traditional simple methods. For instance, at focus, this makes the focal spot bigger, hence preventing the detection of tiny deformations due to chromatic effects.

Yet, the effect is very clear on the INSIGHT results. By subtracting the wavefront profiles obtained at each frequency, we indeed observe the additional frequency-dependent horizontal wavefront tilt resulting from the grating rotation (lower line). From one measurement to the next, all wavefront defects almost perfectly cancel out, leaving only the additional effect originating from the grating rotation. The quantitative analysis provided in the main text show that this angular dispersion corresponds to the theoretically expected value. This not only demonstrates the validity and reliability of INSIGHT, but also tests its reproducibility from one measurement to the next.

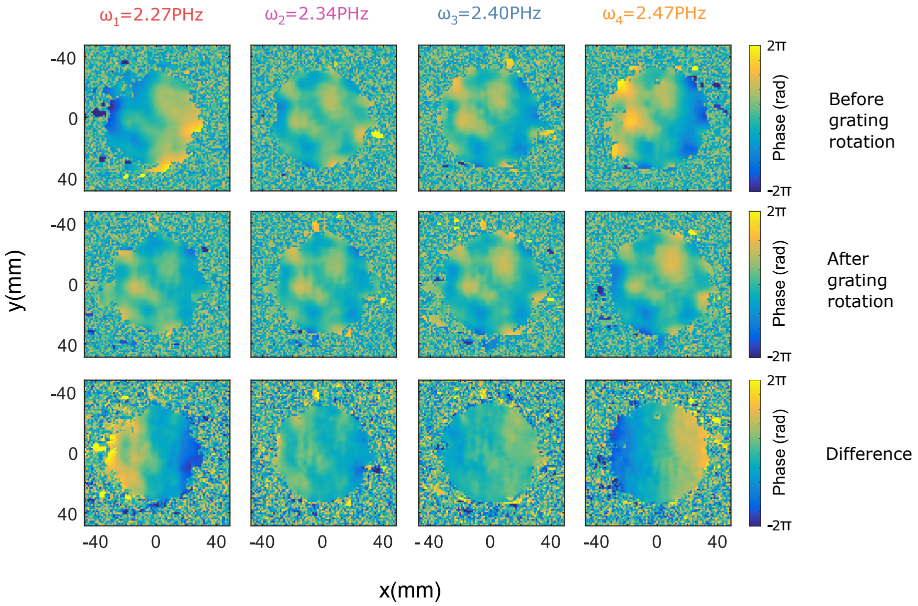

Fig. 11. Color maps of frequency-resolved wavefronts of the collimated UHI100 laser beam at four different frequencies, measured with INSIGHT before (upper line) and after (middle line) a rotation of a compressor grating by $16 \times 10^{-3}$ degrees. The lower line shows the difference between the two cases for each frequency, and clearly reveals the additional frequency-dependent wavefront tilt induced on the beam by the grating rotation.

## Funding

European Research Council (ERC) (grant ExCoMet number 694596); Investissements d'Avenir LabEx PALM (ANR-10-LABX-0039-PALM, EXYT and IMAPS grants); CEA-DRF (DRF-Impulsion funding program).

## Acknowledgments

The authors gratefully acknowledge Manuel Joffre for fruitful discussions on Fourier-transform spectroscopy and its subtleties, as well as Olivier Gobert and Spencer Jolly for their help and Fabrice Réau, Christophe Pothier and David Garzella for operating the UHI100 laser source.